Electronic Supplementary Information for:

A Zn Based Coordination Polymer Exhibiting Long-Lasting Phosphorescence

Javier Cepeda, Eider San Sebastian, Daniel Padro, Antonio Rodríguez-Diéguez, Jose A. García, Jesus M. Ugalde, and Jose M. Seco

Contents:

S1. Materials and Measurements.

All chemicals were of reagent grade and were used as commercially obtained. Thermal analysis (TG/DTA) was performed on a TA Instruments SDT 2960 thermal analyser from room temperature up to 800 ºC in a synthetic air atmosphere (79% N_2 / 21% O_2) with a heating rate of 5 ºC/min. Elemental analyses (C, H, and N) were performed on a Fisons Instruments EA-1008 analyser. Metal content was determined by inductively coupled plasma (ICP-AES) analysis with a Horiba Yobin Yvon Activa spectrometer. The IR spectrum (KBr pellets) was recorded on a ThermoNicolet IR 200 spectrometer in the 4000−400 cm^{-1} spectral region.

X-ray powder diffraction (XRPD) pattern was collected on a Phillips X'PERT powder diffractometer with Cu-Kα radiation (λ = 1.54060 Å) over the 5 < 2θ < 50º range with a step size of 0.026º and an acquisition time of 2.5 s per step at 25 ºC. Indexation of the diffraction profiles were made by means of the FULLPROF program (pattern-matching analysis) on the basis of the space group and the cell parameters found for compound **1** with single crystal X-ray diffraction.

S2. X-ray Data Collection and Structure Determination.

X-ray data collection of a suitable single crystal of **1** was done at 100(2) K on a Bruker VENTURE area detector equipped with graphite monochromated Mo-Kα radiation (λ = 0.71073 Å) by applying the ω-scan method. The data reduction was performed with the APEX2[1] software and corrected for absorption using SADABS.[2] Crystal structure was solved by direct methods using the SIR97 program[3] and refined by full-matrix least-squares on F^2 including all reflections and using anisotropic displacement parameters by means of the WINGX crystallographic package.[4] Hydrogen atoms belonging to the 6ani ligand were located in the difference Fourier map and included as fixed contributions riding on attached atoms with isotropic thermal displacement parameters 1.2 times those of their parent atoms. The structure refinement converges with the Flack parameter equal to 0.45, which seems to indicate that a partial mixture of enantiomers is present. CCDC 1473389 contains the supplementary crystallographic data for this

[1] Bruker Apex2, Bruker AXS Inc., Madison, Wisconsin, USA, 2004.
[2] G.M. Sheldrick, SADABS, Program for Empirical Adsorption Correction, Institute for Inorganic Chemistry, University of Gottingen, Germany, 1996.
[3] A. Altomare, M. C. Burla, M. Camilla, G. L. Cascarano, C. Giacovazzo, A. Guagliardi, A. G. G. Moliterni, G. Polidori and R. Spagna, *J. Appl. Cryst.*, 1999, **32**, 115.
[4] (a) G. M. Sheldrick, SHELX-2014, Program for Crystal Structure Refinement, University of Göttingen, Göttingen, Germany, 2014. (b) L. J. Farrugia, *J. Appl. Cryst.*, 1999, **32**, 837.

communication. These data can be obtained free of charge via http://www.ccdc.cam.ac.uk/conts/retrieving.html (or from the Cambridge Crystallographic Data Centre, 12, Union Road, Cambridge CB2 1EZ, UK; fax: +44 1223 336033). Crystallographic data are summarised in Table S1.

Table S1. Crystallographic data and structure refinement details of compound **1**.

	1		**1**
Empirical formula	$C_{12}H_{19}N_4O_4Zn$	ρ (g cm^{-3})	1.630
Formula weight	339.61	Crystal size (mm^3)	0.32 x 0.25 x 0.18
Crystal system	Tetragonal	F(000)	688
Space group	$P4_32_12$	Unique reflections / total	1796 / 13404
a (Å)	7.8691(7)	GOF	1.235
b (Å)	7.8691(7)	R_{int}	0.0282
c (Å)	22.353(3)	Final R indices	
V (Å^3)	1384.1(3)	R_1[a] / wR_2[b] [I>2σ(I)]	0.0494 / 0.1038
Z	4	R_1[a] / wR_2[b] (all data)	0.0525 / 0.1047
μ (mm^{-1})	1.795		

[a] $S = [\sum w(F_0^2 - F_c^2)^2 / (N_{obs} - N_{param})]^{1/2}$. [b] $R_1 = \sum||F_0|-|F_c|| / \sum|F_0|$. [c] $wR_2 = [\sum w(F_0^2 - F_c^2)^2 / \sum wF_0^2]^{1/2}$; $w = 1/[\sigma^2(F_0^2) + (aP)^2]$ where $P = (\max(F_0^2,0) + 2F_c^2)/3$ with a = 5.9161.

Table S2. Selected bond lengths for compound **1**.[a]

Zn1–N1	2.059(4)	Zn1–O1(ii)	1.963(4)
Zn1–N1(i)	2.059(4)	Zn1–O1(iii)	1.963(4)

[a] Symmetries: (i) –y + 3/2, x + 3/2, z + 7/4; (ii) x, y – 1, z; (iii) –y + 5/2, x + 3/2, z + 7/4.

Table S3. Hydrogen bonding interactions (Å, º) of compound **1**.[a]

D–H···A[b]	*D–H*	*H···A*	*D···A*	*D–H···A*
N8–H81···O1(ii)	0.86	1.96	2.784(13)	159.5
N8–H82···O2(iv)	0.86	2.26	2.824(13)	123.5

[a] Symmetry codes: (iv) –y + 3/2, x – 1/2, z – 1/4. [b] D: donor. A: acceptor.

Table S4. Structural parameters (Å, º) of *π*–*π* interactions of compound **1**.[a]

Ring···Ring[b]	α	DC	β	DZ	Dist.
1A–1A(v)	32.82	4.269(3)	39.20	4.24	3.26–3.56
1A–1A(vi)	32.82	4.269(3)	6.53	3.31	3.26–3.56

[a] Symmetry: (v) x – 1/2, –y + 3/2, –z + 5/4; (vi) x + 1/2, –y + 3/2, –z + 5/4. α: dihedral angle between mean planes of the rings (°), DC: distance between ring centroids (Å), β: angle between DC vector and normal to plane(I) (°), DZ: perpendicular distance of the centroids of ring(I) on plane of ring(II) (Å), Dist.: shorter distances between non-hydrogen atoms of rings (I) and (II). [b] Rings: **1A**: N1, C2, C3, C4, C5, C6.

S3. Synthesis of 1.

5 mL of an aqueous solution containing 0.1 mmol of $Zn(NO_3)_2 \cdot 6H_2O$ (0.0298 g) were added dropwise over an aqueous/methanol (20 mL, 1:1) solution of 0.2 mmol of H6ani (0.0276 g) under continuous stirring at 70 ºC. Then, 1 mL of triethylamine (>98%) was added dropwise to the reaction mixture, such that the final pH of the solution was 6.4 and a white precipitate corresponding to compound **1** was obtained. The suspension was cooled down, the precipitate filtered off and mother liquors were left to slowly evaporate at room temperature. Well shaped antiprismatic single crystals were grown 5 months later, which were collected by filtration and washed several times with water and methanol. Compound **1** has the $[Zn(\mu\text{-}6ani)_2]_n$ formula based on X-ray single crystal, elemental and thermogravimetric analyses. Elemental analysis for $C_{12}H_{19}N_4O_4Zn$ (339.61 g mol^{-1}). Calcd.: C, 41.33; H, 5.49; N, 16.07; Zn, 18.75. Found: C, 41.61; H, 5.38; N, 15.89; Zn, 18.93.

S4. Photoluminescence measurements.

Lifetime, Time Resolved Emission Spectroscopy (TRES) and steady state photoluminescence (PL) were measured on crystalline samples from 10 K to room temperature using a closed cycle helium cryostat enclosed in an Edinburgh Instruments FLS920 spectrometer. For steady state measurements an IK3552R-G HeCd continuous laser (325 nm) and a Müller-Elektronik- Optik SVX1450 Xe lamp were used as excitation source. Single-crystal emission spectra and photographs were obtained at room temperature in a micro-PL system included in an Olympus optical microscope illuminated with a HeCd laser or a Hg lamp.

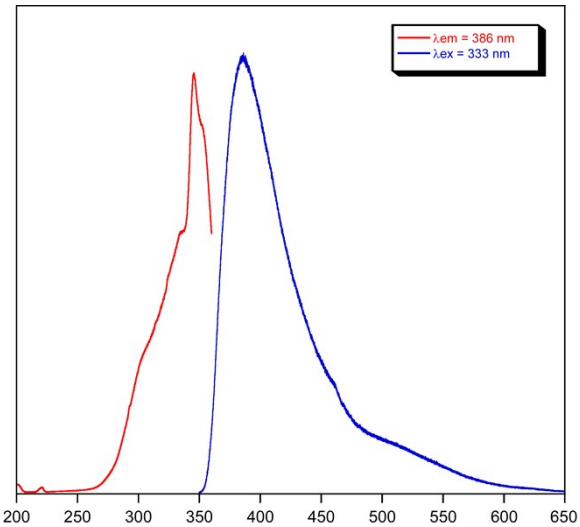

Figure S1. Excitation and emission spectra of the H6ani ligand.

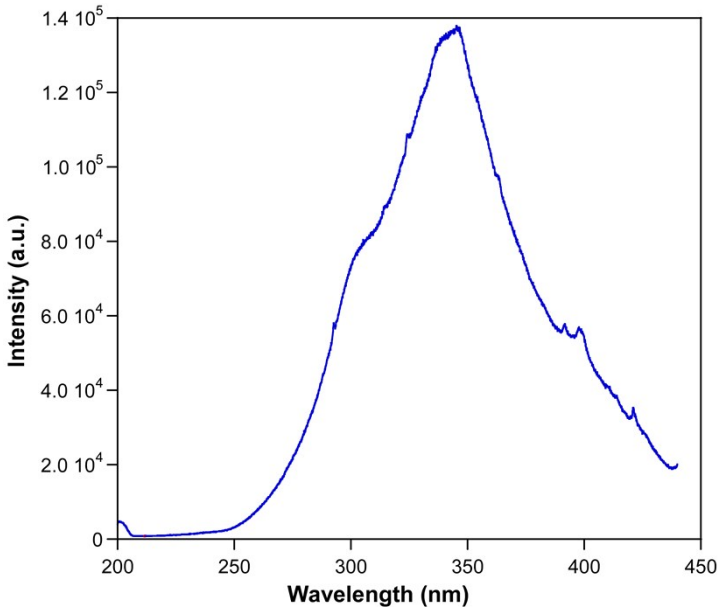

Figure S2. Excitation spectrum of **1** monitored at the 461 nm emission line.

Emission spectra of compound **1** were performed at different temperatures in order to check whether it shows thermochromic behaviour. However, as inferred from Figure S3, the emission of the compound is almost unchanged with the temperature. As expected, the only difference is a less emission intensity according with the increasing temperature.

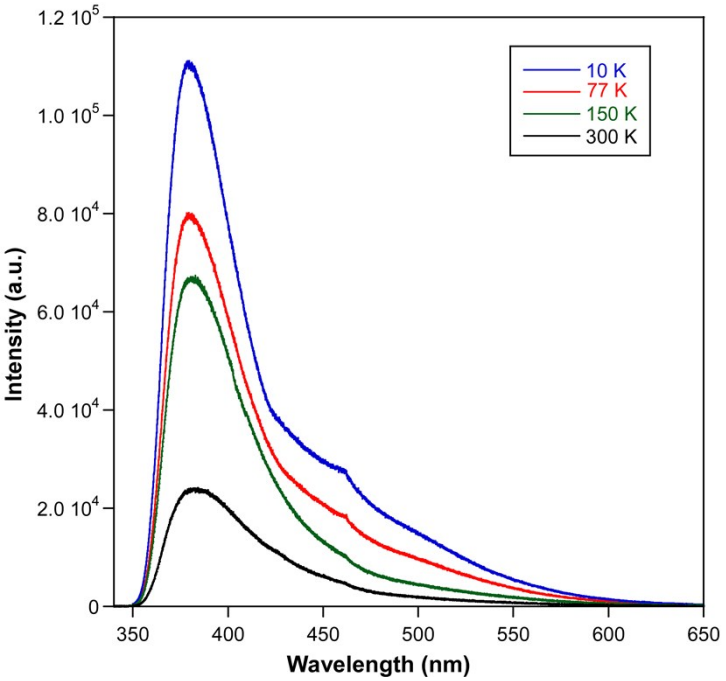

Figure S3. Emission spectra of **1** under excitation at 333 nm at different temperatures.

S5. Thermogravimetric Analysis.

A plateau in the TG curve from room temperature up to 400 ºC is observed in good agreement with the lack of solvent molecules in the crystal structure of compound **1**. This fact, together with the absence of DTA peaks stands for the robustness of its crystal building as a result of the strong supramolecular interactions among the Zn-6ani layers in the three-dimensional packing. Above 400 ºC, compound **1** experiments several exothermic processes as a consequence of the decomposition of the organic part, leading to ZnO as a final residue.

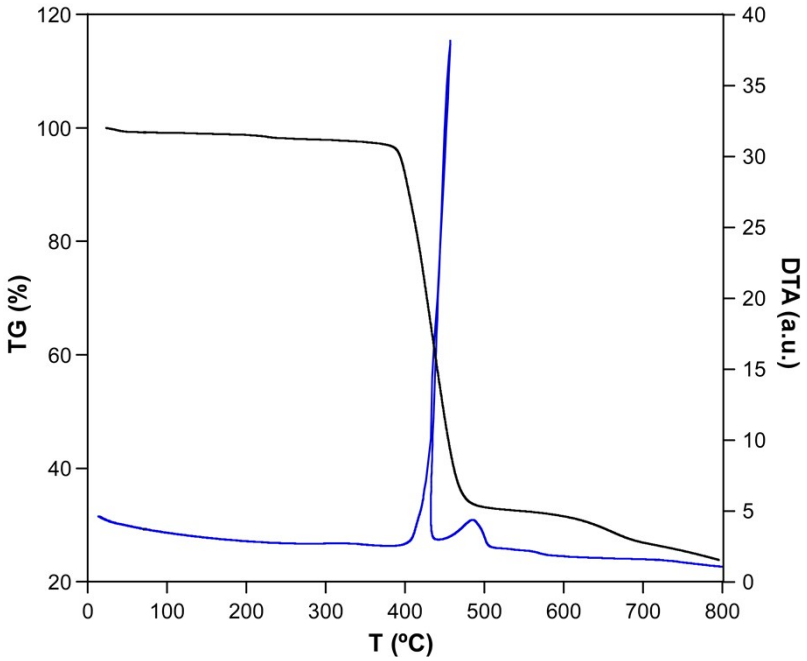

Figure S4. TG/DTA analysis for compound **1**.

S6. Powder X-ray Diffraction Analysis.

Pattern-matching analysis confirms the purity of the polycrystalline sample of **1**.

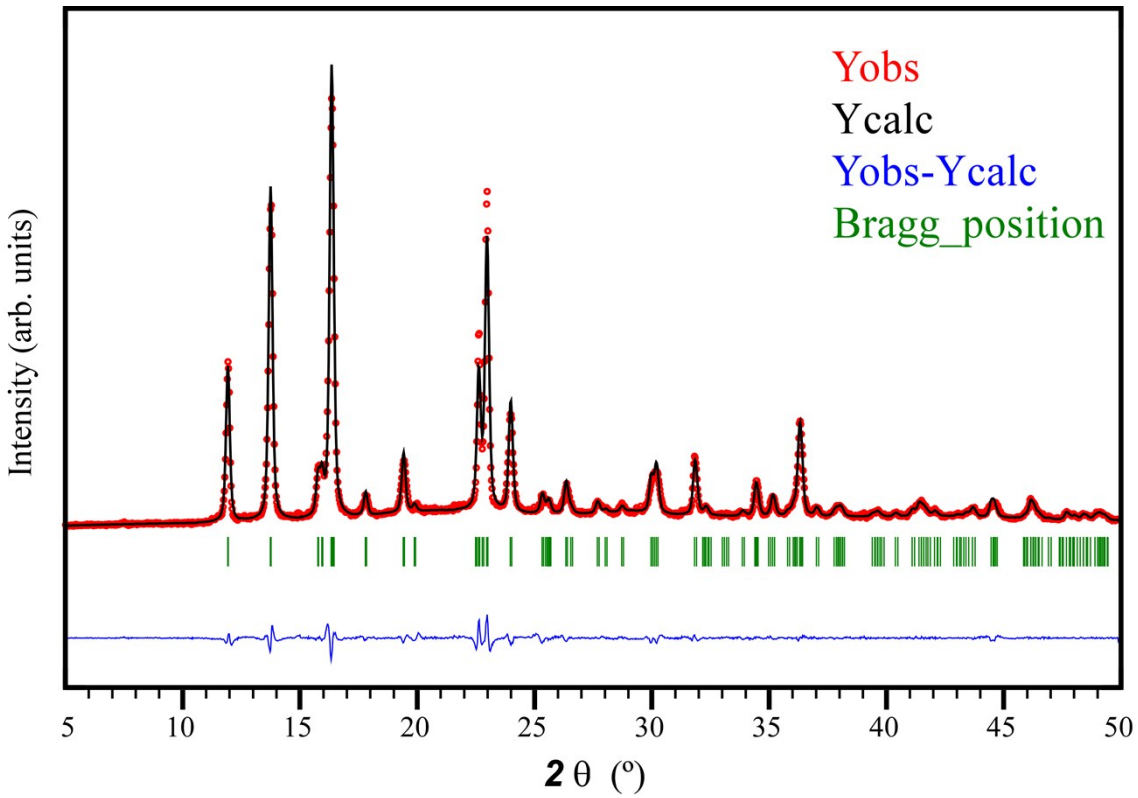

Figure S5. Pattern-matching analysis of polycrystalline sample of compound **1**.

S7. FT-IR spectroscopy.

FTIR spectrum of **1** has been assigned according to bibliography and the frequency modes derived from a DFT-optimized model of the molecule. At high frequencies, spectrum of **1** exhibits an intense band at 3460 cm^{-1} that corresponds to the vibration of the O–H bond of free water of moisture, followed by strong vibrations at 3320 and 3220 cm^{-1} related with exocyclic amino group. Weak shoulders between 3100 and 2900 cm^{-1} are attributed to C–H vibrations of the pyridinic ring of the ligand. The intense vibrations in the 1660–1520 cm^{-1} region correspond to both the asymmetric stretching vibrations of the carboxylate groups and the aromatic C–C and C–N bonds, while the symmetric stretching vibrations of the carboxylate groups occur in the lower range of 1390–1270 cm^{-1}. At lower frequencies, the remaining bands are assigned to the distortions originated in the aromatic ring and the carboxylate groups of the 6ani ligand. The vibration bands of the Zn–O and Zn–N bonds are observed around 530 cm^{-1}.

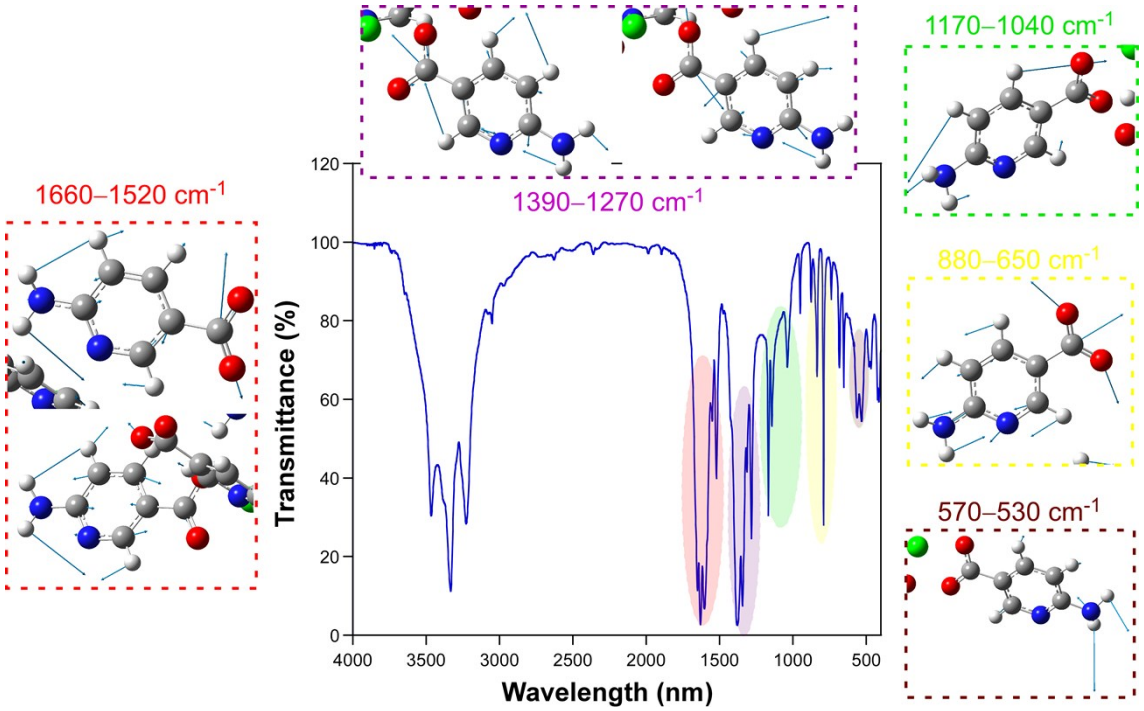

Figure S6. FTIR spectrum of compound **1** together with the normal vibration modes.

S8. Lifetime measurements.

Lifetime measurements were initially performed at 10 K over the polycrystalline sample under excitation at the maximum (333 nm) for selected emission wavelengths in the 350–650 nm range. The decay curves were recorded employing different exposure times in order to achieve 10^4 counts in the pulse of reference. Given the fluorescent (380 and 400 nm) and phosphorescent (425–600) emissions according to the wavelength, nanosecond or microsecond pulse lamps were employed when appropriate. On the one hand, fitting results corresponding to the decay curves of 380 and 400 nm were obtained by deconvoluting the pulse signal according to Intrument Response Functions (IRF) at the same working conditions. On the other hand, the remaining decay curves were analyzed by tail fitting.

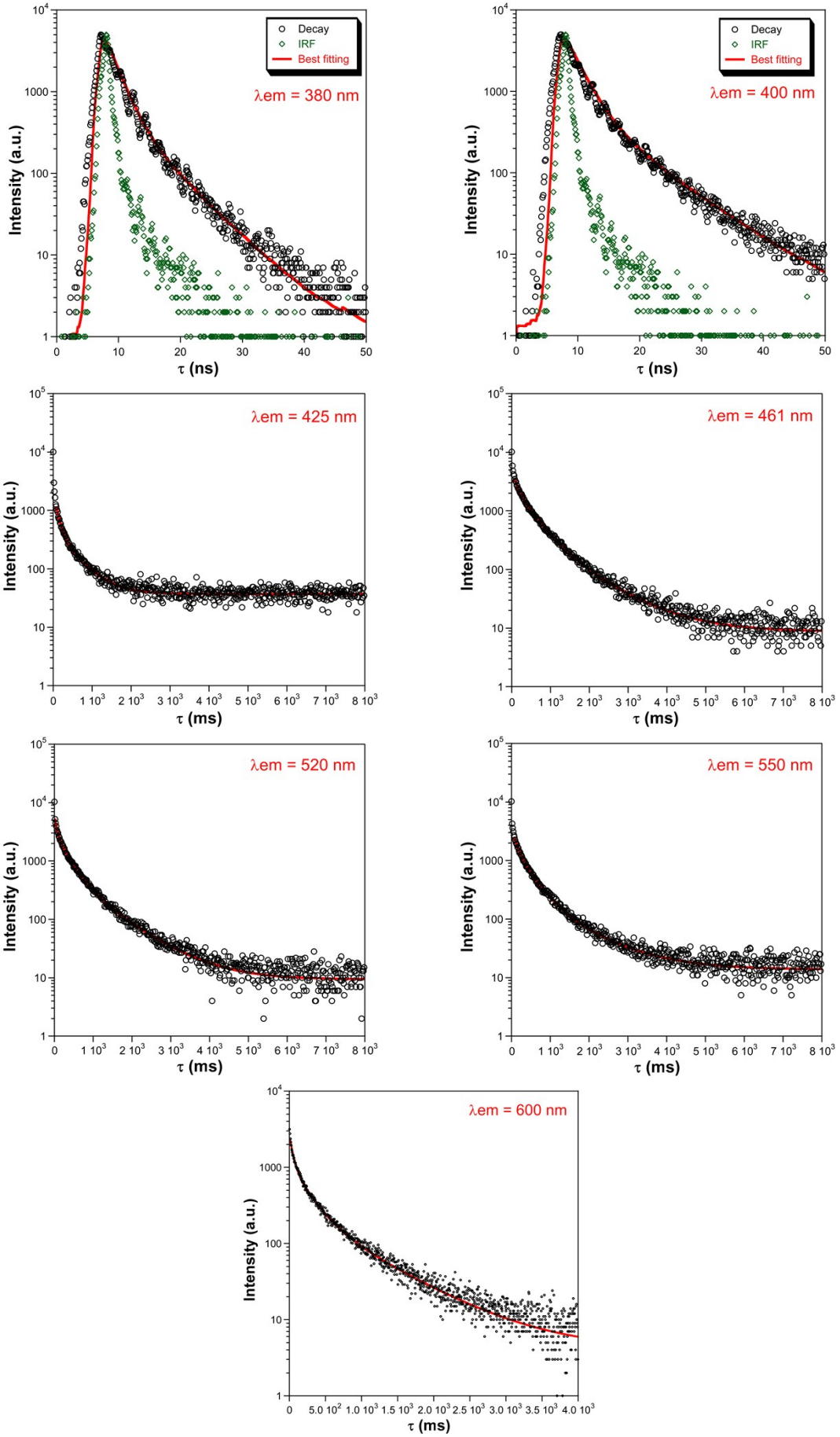

Figure S7. Emission decay curves showing the best fitting.

Table S5. Best fit results of decay curves performed at 10K monitoring emission wavelengths on the maxima.

Wavelength (nm)	τ_1 (ns)	Chi Sq.
380	5.8(1)	1.777
400	6.8(1)	1.613

Table S6. Best fit results of decay curves performed at 10K monitoring different emission wavelengths.

Wavelength (nm)	τ_1 (ms)	τ_2 (ms)	τ_3 (ms)	Chi Sq.
425	38(2) / 14%	192(12) / 39%	702(28) / 47%	1.702
461	118(12) / 12%	426(30) / 55%	1070(69) / 33%	1.329
491	43(3) / 5%	232(8) / 34%	800(14) / 61%	1.349
520	63(4) / 12%	308(13 / 48%	928(27) / 40%	1.359
550	106(18) /12%	377(29) / 56%	1117(85) / 32%	1.630
575	44(4) / 10%	242(11) / 49%	834(29) / 41%	1.736
600	60(3) / 15%	264(15) / 43%	875(46) / 42%	1.731

Additionally, variable-temperature measurements were performed at the 461 nm (small peak in the continuous spectrum and main phosphorescent component according to the TRES) since it is the wavelength associated with the longest lifetime. As shown in Table S7, the longest lifetime slowly decreases with rising the temperature.

Table S7. Best fit results of decay curves performed at 10K monitoring different emission wavelengths.

Temperature (K)	τ_1 (ms)	τ_2 (ms)	τ_3 (ms)	Chi Sq.
10	118(12) / 12%	426(30) / 55%	1070(69) / 33%	1.329
25	118(10) / 14%	445(25) / 58%	1184(77) / 28%	1.650
50	92(13) / 5%	401(21) / 46%	1013(26) / 49%	1.394
75	73(7) / 8%	360(16) / 53%	989(34) / 39%	1.772
100	96(13) / 12%	327(23) / 56%	973(54) / 32%	1.865
150	95(13) / 12%	327(22) / 56%	973(43) / 32%	1.865
200	58(5) / 44%	290(25) / 56%	–	1.981

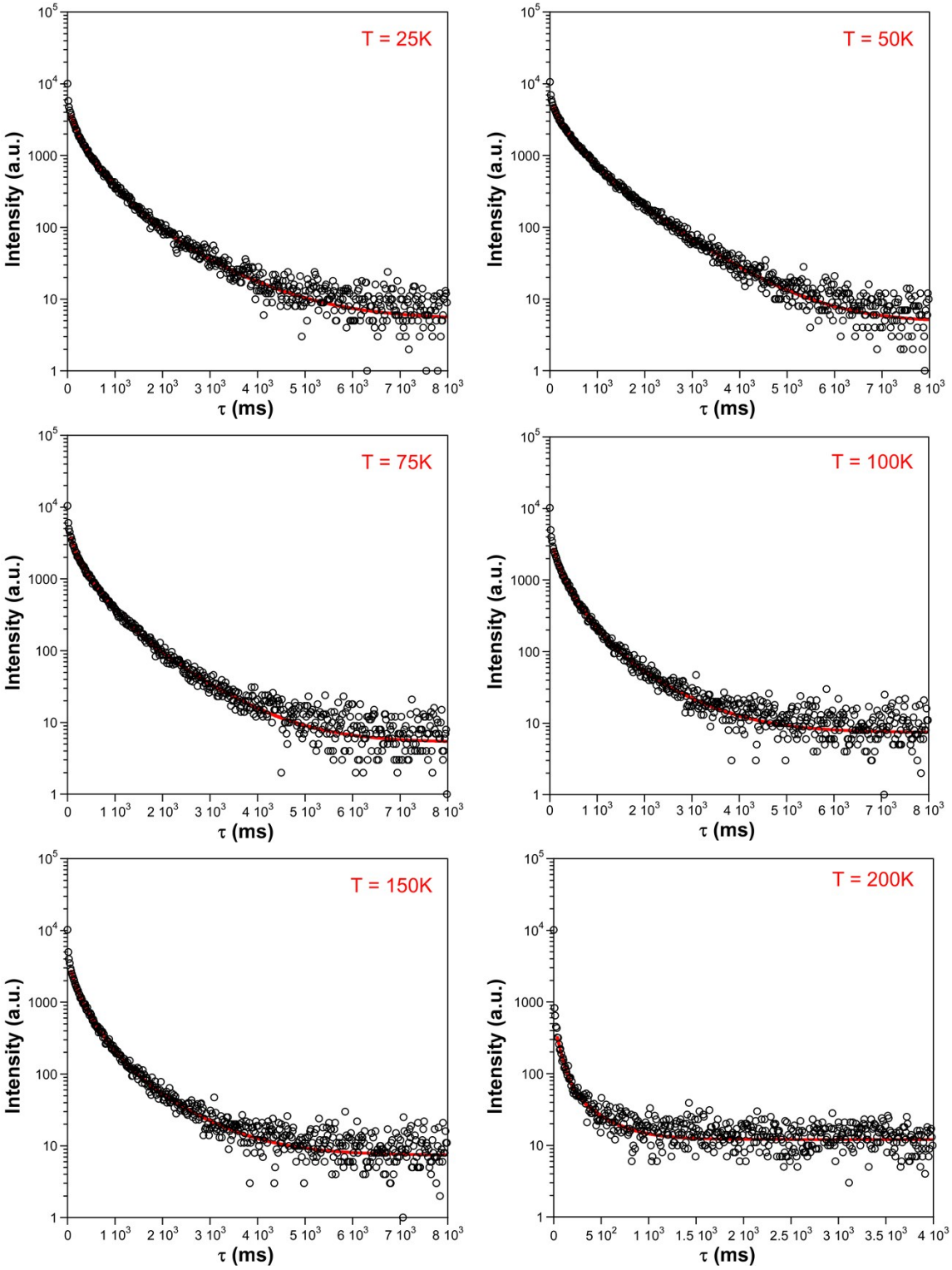

Figure S8. Variable-temperature decay curves at 461 nm showing the best fitting.

S9. TD-DFT computational details.

TD-DFT theoretical calculations were performed at 10K using the Gaussian 09 package,[5] using the Becke three parameter hybrid functional with the non-local correlation functional of Lee-Yang-Parr (B3LYP)[6] for all atoms but for the central zinc cation, where the LANL2DZ[7] basis set along with the corresponding effective core potential (ECP) was used, whereas 6-31G(d)[8] was adopted for the remaining atoms. The latter has been proven to be an adequate method to describe luminescence of zinc based coordination compounds.[9] A suitable model of **1** (model **1** hereafter, Figure S9) was built from the X-ray single crystal structure of **1**, which consists of an excerpt with the ligands whose donor atoms establish the first coordination sphere of the metal. The inclusion of potentially important π-π stacking interactions (see model **2** in Figure S10) did not improve the theoretical results (data not shown). The 40 lowest excitation and emission energies were calculated on model **1** by the TD-DFT method. Gaussian results were analyzed using the GaussSum program package[10] and molecular orbitals plotted using GaussView 5.[11]

[5] M. J. Frisch, G. W. Trucks, H. B. Schlegel, G. E. Scuseria, M. A. Robb, J. R. Cheeseman, G. Scalmani, V. Barone, B. Mennucci, G. A. Petersson, H. Nakatsuji, M. Caricato, X. Li, H. P. Hratchian, A. F. Izmaylov, J. Bloino, G. Zheng, J. L. Sonnenberg, M. Hada, M. Ehara, K. Toyota, R. Fukuda, J. Hasegawa, M. Ishida, T. Nakajima, Y. Honda, O. Kitao, H. Nakai, T. Vreven, J. A. Montgomery Jr., J. E. Peralta, F. Ogliaro, M. Bearpark, J. J. Heyd, E. Brothers, K. N. Kudin, V. N. Staroverov, R. Kobayashi, J. Normand, K. Raghavachari, A. Rendell, J. C. Burant, S. S. Iyengar, J. Tomasi, M. Cossi, N. Rega, J. M. Millam, M. Klene, J. E. Knox, J. B. Cross, V. Bakken, C. Adamo, J. Jaramillo, R. Gomperts, R. E. Stratmann, O. Yazyev, A. J. Austin, R. Cammi, C. Pomelli, J. W. Ochterski, R. L. Martin, K. Morokuma, V. G. Zakrzewski, G. A. Voth, P. Salvador, J. J. Dannenberg, S. Dapprich, A. D. Daniels, O. Farkas, J. B. Foresman, J. V. Ortiz, J. Cioslowski and D. J. Fox, Gaussian 09, revision A.02, Gaussian, Inc., Wallingford, CT, 2009.

[6] (a) A. D. Becke, *J. Chem. Phys.*, 1993, **98**, 5648. (b) B. Miehlich, A. Savin, H. Stoll and H. Preuss, *Chem. Phys. Lett.*, 1989, **157**, 200. (c) C. Lee, W. Yang and R. G. Parr, *Phys. Rev. B*, 1988, **37**, 785.

[7] (a) P. J. Hay and W. R. Wadt, *J. Chem. Phys.*, 1985, **82**, 270. (b) W. R. Wadt and P. J. Hay, *J. Chem. Phys.*, 1985, **82**, 284. (c) P. J. Hay and W. R. Wadt, *J. Chem. Phys.*, 1985, **82**, 299.

[8] (a) V. A. Rassolov, M. A. Ratner, J. A. Pople, P. C. Redfern and L. A. Curtiss, *J. Comput. Chem.*, 2001, **22**, 976. (b) M. M. Francl, W. J. Pietro, W. J. Hehre, J. S. Binkley, D. J. DeFrees, J. A. Pople and M. S. Gordon, *J. Chem. Phys.*, 1982, **77**, 3654. (c) P. C. Hariharan and J. A. Pople, *Mol. Phys.*, 1974, **27**, 209.

[9] (a) X. Shuhong, W. Chunlei, W. Zhuyuan and C. Yiping, *J. Mol. Mod.,* 2014, **20**, 1. (b) Z. Kangcheng, L. Xuewen, D. Hong, C. Hui, Y. Fengcun and J. Liangnian, *J. Mol. Struc.: THEOCHEM*, 2003, **626**, 295.

[10] N. M. O'Boyle, A. L. Tenderholt and K. M. Langner, *J. Comput. Chem.*, 2008, **29**, 839.

[11] GaussView, Version 5, R. Dennington, T. Keith and J. Millam, *Semichem Inc.*, Shawnee Mission, KS, 2009.

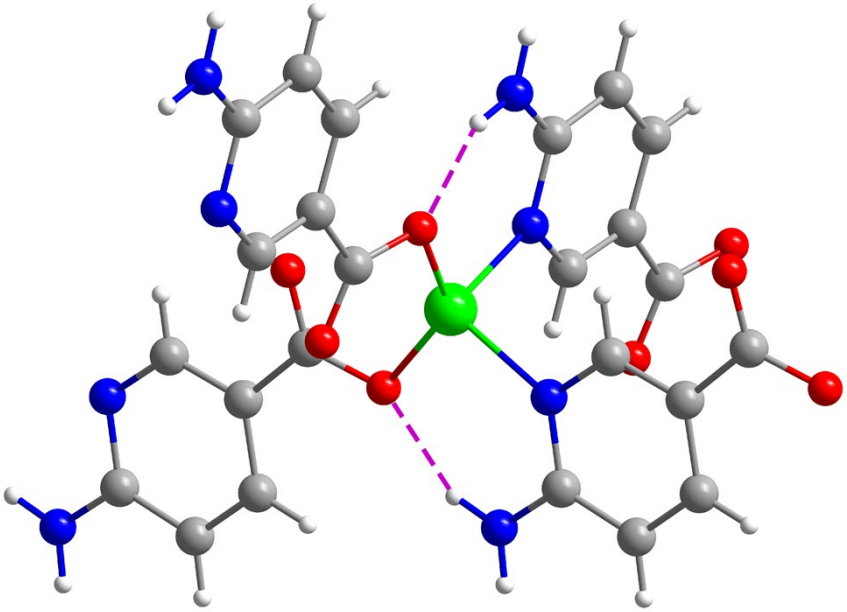

Figure S9. Molecular excerpt used as model **1** for the calculations.

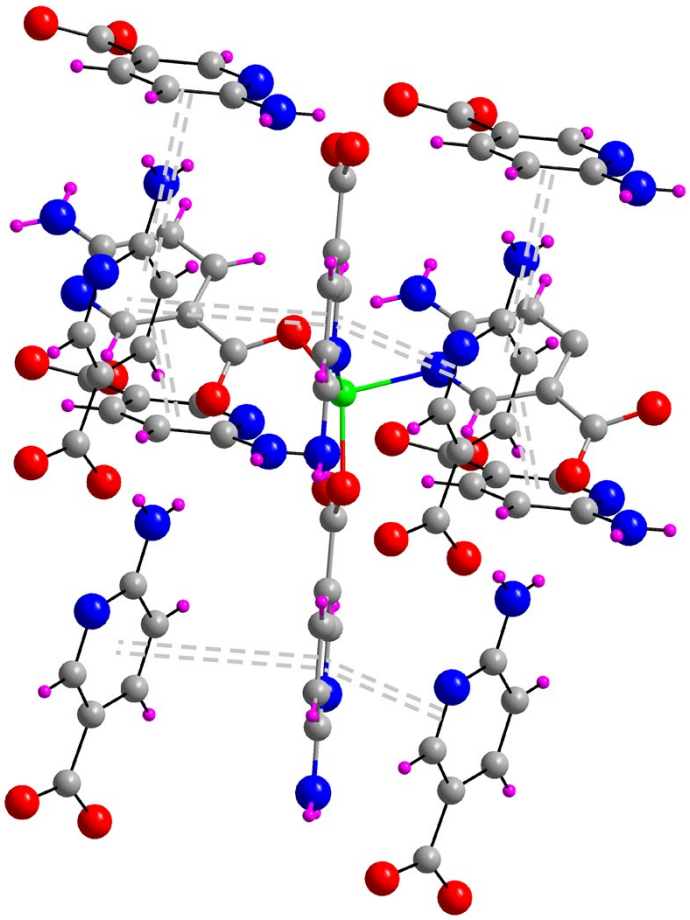

Figure S10. Molecular excerpt used as model **2** for the calculations.

Table S8. Calculated main excitation energies (nm) and electronic transitions of model **1** in gas phase.

Calcd. λ (nm)	Exp. λ (nm)	Significant contributions
345	333	HOMO → LUMO + 8 (36%) HOMO – 1 → LUMO + 9 (24%) HOMO – 1 → LUMO + 7 (14%) HOMO – 4 → LUMO + 3 (11%) HOMO – 5 → LUMO + 2 (7%) HOMO – 5 → LUMO
375	–	HOMO → LUMO + 6 HOMO → LUMO + 5 HOMO → LUMO + 7

Table S9. Calculated main emission energies (nm) and electronic transitions of model **1** in gas phase.

Calcd. λ (nm)	Exp. λ (nm)	Significant contributions
376	380	HOMO – 4 → LUMO + 4 (91%) HOMO – 3 → LUMO + 4 (6%)
369–370	380	HOMO – 4 → LUMO + 4 (99%)
404	430	HOMO – 1 → LUMO + 5 (99%)
467	460	HOMO → LUMO + 6 (91%) HOMO → LUMO + 9 (3%)
470–495	–	HOMO – 1 → LUMO + 5 (99%)
548		HOMO → LUMO + 6 (88%) HOMO → LUMO + 4 (8%)
582	–	HOMO → LUMO + 7 (76%) HOMO → LUMO + 4 (12%) HOMO → LUMO + 6 (9%)

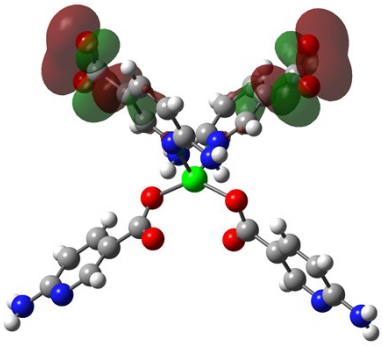

HOMO – 5

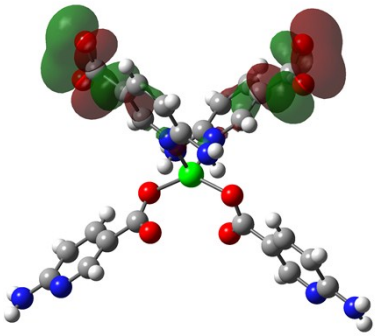

HOMO – 4

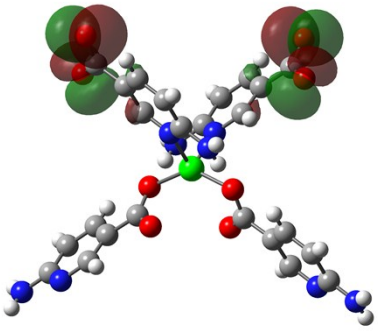

HOMO – 1

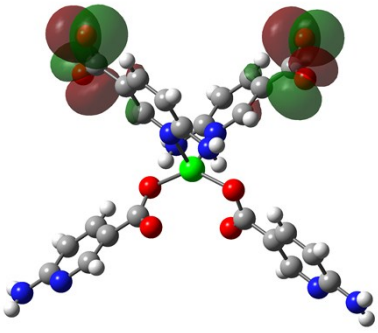

HOMO

Figure S11. Highly Occupied Molecular Orbitals of ground state of model **1** involved in the luminescent charge transitions.

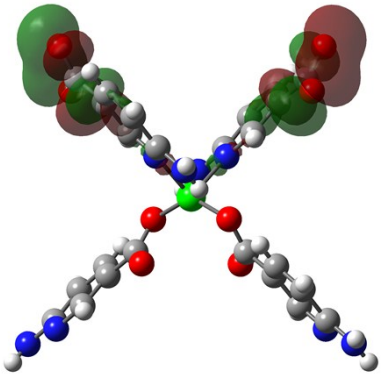

HOMO – 4

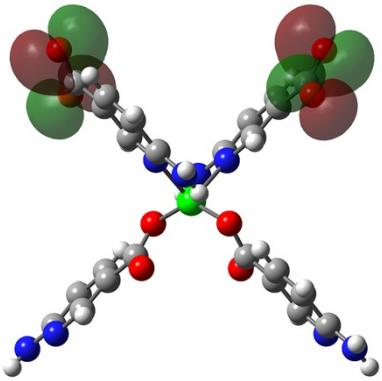

HOMO –3

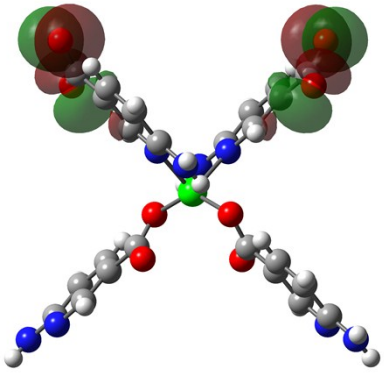

HOMO – 1

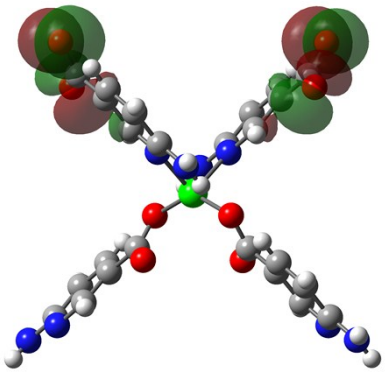

HOMO

Figure S12. Highly Occupied Molecular Orbitals of excited state of model **1** involved in the luminescent charge transitions.

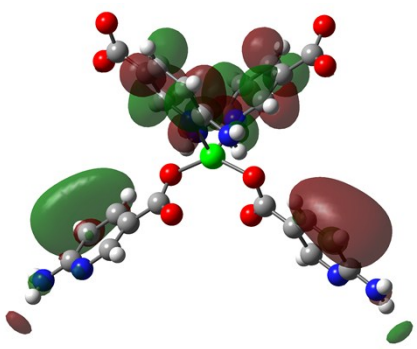

LUMO + 9

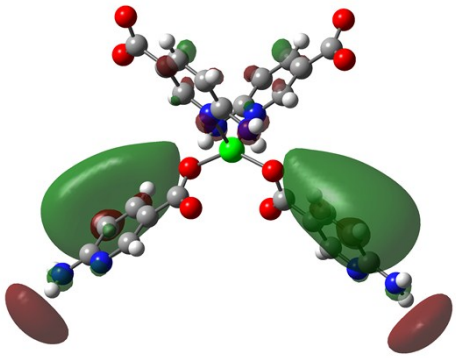

LUMO + 8

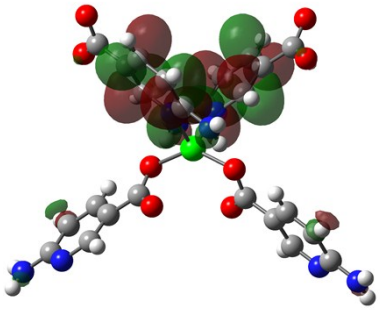

LUMO + 7

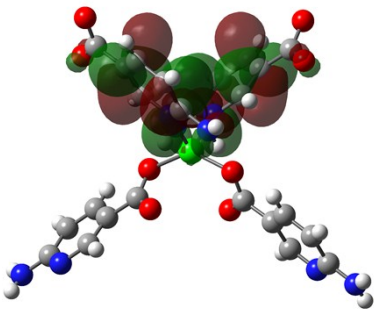

LUMO + 6

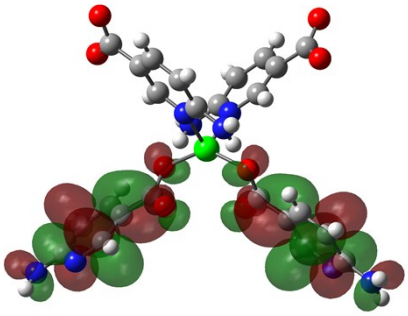

LUMO + 5

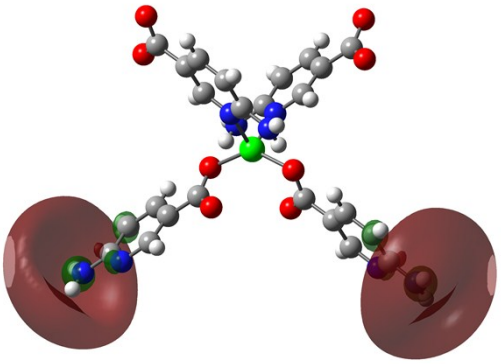

LUMO + 3

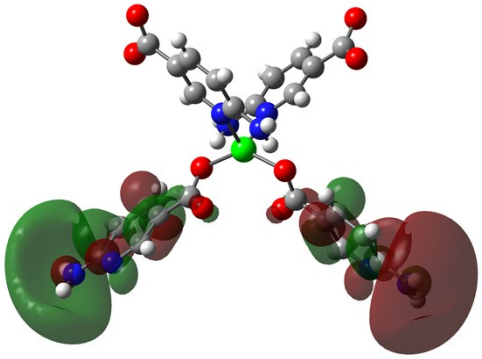

LUMO + 2

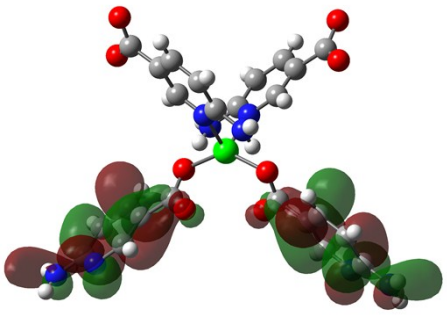

LUMO

Figure S13. Lowest Unoccupied Molecular Orbitals of ground state of model **1** involved in the luminescent charge transitions.

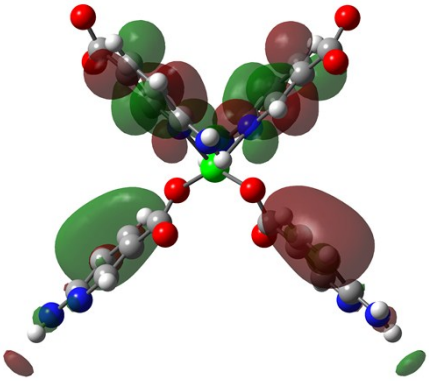

LUMO + 9

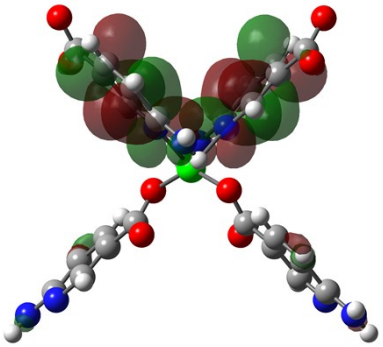

LUMO + 7

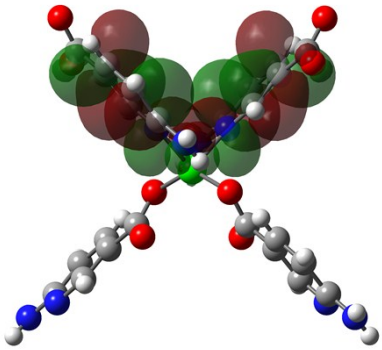

LUMO + 6

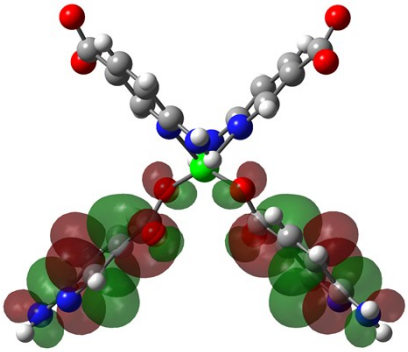

LUMO + 5

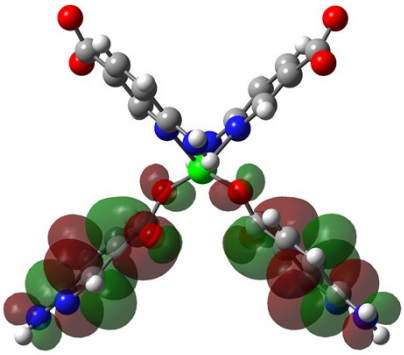

LUMO + 4

Figure S14. Lowest Unoccupied Molecular Orbitals of excited state of model **1** involved in the luminescent charge transitions.

S10. Time-resolved emission spectra.

TRES measurement was performed for the whole emission spectrum with a step of 5 nm and 0.5 Hz of frequency at the pulsed lamp. Each spectrum has been deconvoluted according to the standard colour system and plotted in the chromaticity CIE 1931 diagram.

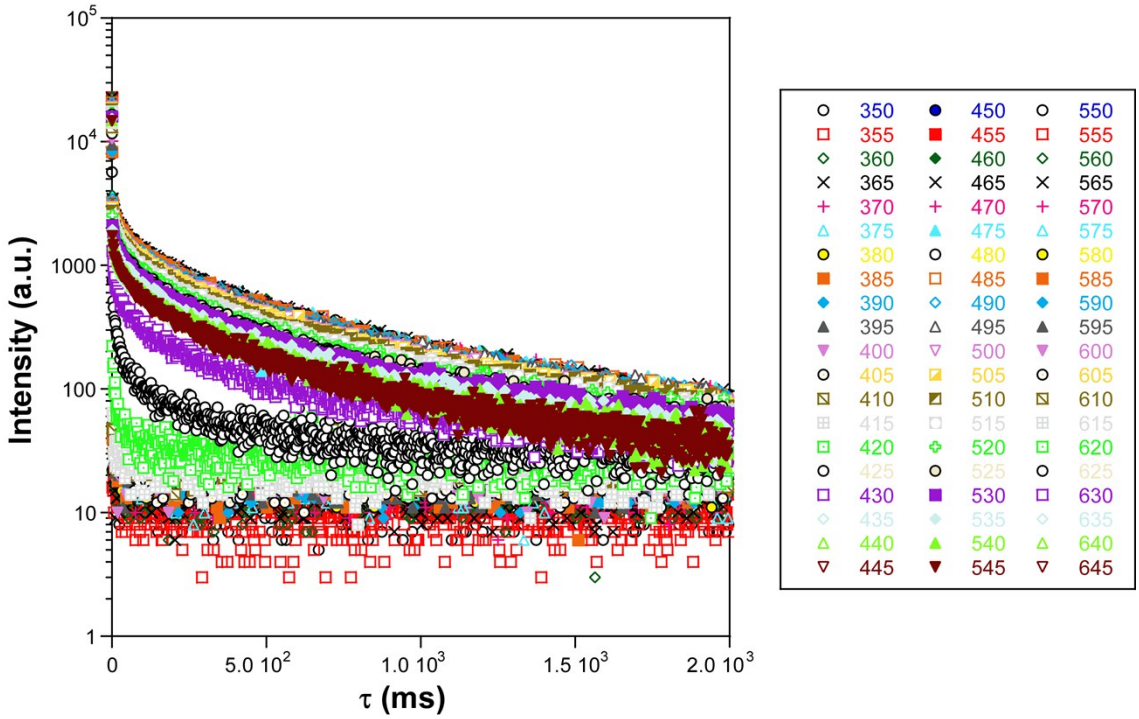

Figure S15. Time-resolved emission spectra in the 350–650 nm region.